Temperature Controlled Terahertz Absorbers based on Omega Resonators

Jia-Tong Jing[1], Wei Song[1], Ting-Ting Ge[1], Xin-Qing Sheng[1], Aliaksei Balmakou[2], and Sergei Khakhomov[2]

[1]Institute of Radio Frequency Technology and Software
Beijing Institute of Technology, Beijing, 100081, China
3120215362@bit.edu.cn, wsong@bit.edu.cn, 18810669611@163.com, xsheng@bit.edu.cn

[2]Departments of Optics
Francisk Skorina Gomel State University, Gomel, 246028, Belarus
balmakou@gmail.com, khakh@gsu.by

***Abstract* –** In this article, the structural stability of a metasurface absorber that works at 2.8 THz is analyzed. Since the absorber is made of metallic titanium, its elemental inclusions will be heated up and expand when absorbing electromagnetic waves. To evaluate the accumulated heat, the structural thermal expansion and the stability of the wave-absorbing performance, electromagnetism-thermodynamics-structural mechanics multiphysics simulations are conducted. Based on the thermal stability study, thermistors are further introduced into the metasurface, leading to two thermal controlled terahertz absorbers. Numerical experiments show that the absorbers present a peak absorption coefficient of 92.7% at 2.79 THz up to the temperature of 1761.4 K. When the temperature rises, the absorption frequencies of the two absorbers shift to 3.51 THz and 3.94 THz, with the peak absorption coefficients of 92.8% and 93.8%, respectively.

***Index Terms* –** multiphysics simulations, thermal controlled terahertz absorbers, thermal expansion.

I. INTRODUCTION

Electrically thin absorbing metasurfaces are of prime importance for many applications, for example, wave filtering [1, 2], radar cross-section reduction [3–6], energy harvesting [7–10], phase modulating [11, 12], and thermal emission control [13–15]. Total absorption of electromagnetic radiation requires elimination of all wave propagation channels: reflection and transmission. The electromagnetic behavior of any arbitrary scatterer may be described by its polarizability tensors [16]. Polarizability tensors determine the linear relation between induced dipole moments and exciting electromagnetic fields. There are various analytical and numerical approaches for calculation of polarizability tensors of scatterers [17–19]. Correspondingly, electrically thin absorbers are proposed [20]. Among these structures, the Ω-shaped metallic resonator is interesting because it demonstrates nearly full absorption for EM waves [21]. Moreover, it can be fabricated by laser lithography methods with subsequent metallization or ion beam-selective etching. So it has potential applications in spatial light modulators, sensors, bolometers and so on [20, 22]. However, there remain two interesting problems.

First, the absorption of electromagnetic waves is based on metallic loss which converts electromagnetic energy into thermal energy. During the process of EM wave absorbing, the heated metal structure may expand. That will affect the polarizability of the metasurface. Especially when metallic contact between the inclusions occurs, the polarizability will be changed dramatically, which would lead to a significant change in the absorbing function of the metasurface absorber. However, to the best of our knowledge, there are few studies on the thermal stability of the absorption.

Second, known from the causality principle, the maximal bandwidth of absorption of a passive absorbing layer is proportional to the layer thickness [23, 24]. So the full absorption of the metasurface exists only in a narrow frequency band, and the band is fixed once the structure of the metasurface is determined. Therefore, dynamically controlling the absorption band remains an interesting topic.

In this paper, we first investigated the thermal stability of a terahertz absorber based on Ω-shaped titanium resonators. An electromagnetism-thermodynamics-structural mechanics multiphysics simulation is conducted. The simulation results show that up to the melting temperature of titanium, the absorber demonstrates stable absorption.

Second, based on the analysis of polarizability, we incorporated thermistors in the Ω resonators and obtained temperature-controlled EM absorbers. In this

Submitted On: April 20, 2023
Accepted On: June 27, 2023

https://doi.org/10.13052/2023.ACES.J.380508

way, the absorption frequency can be shifted by controlling the temperature. Absorption coefficients of over 90% for all the bands are demonstrated in the simulations.

II. METASURFACE ABSORBING THEORY

Consider a metasurface absorber operating at 2.8 THz as proposed in [21]. The metasurface is formed with unit cells in a square lattice, with lattice constants of 37 μm. Each unit cell consists of four pairs of orthogonally arranged Ω-shaped titanium wires as shown in Fig. 1. The diameter of each Ω is 1/7 wavelength.

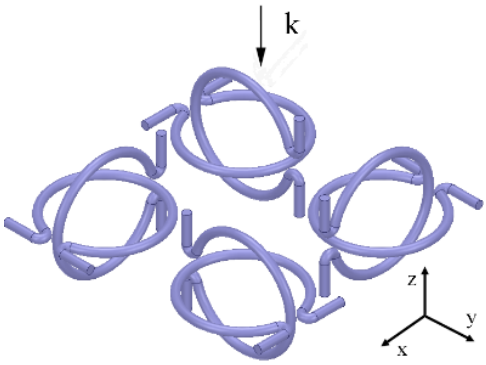

Fig. 1. Schematic of the array of pairs of Ω particles.

Illuminated normally by an incident plane wave, the induced electric and magnetic dipole moments p and m can be modelled with the help of polarizability [16]. Due to the subwavelength dimensions of the array elements, the dipole moments and polarizabilities can be described using the effective surface-averaged values:

$$\begin{bmatrix} p \\ m \end{bmatrix} = \begin{bmatrix} \hat{\alpha}_{ee} & \hat{\alpha}_{em} \\ \hat{\alpha}_{me} & \hat{\alpha}_{mm} \end{bmatrix} \begin{bmatrix} E_{inc} \\ E_{inc} \end{bmatrix}. \tag{1}$$

Here $\hat{\alpha}_{ee}$, $\hat{\alpha}_{em}$, $\hat{\alpha}_{me}$and $\hat{\alpha}_{mm}$are the effective electric, electromagnetic, magnetoelectric and magnetic polarizability tensors of the unit cells.

As shown in [20], the electric fields of the reflected and transmitted waves from this metasurface are given by:

$$E_r = \frac{i\omega}{2S}\left(\eta_0 \hat{\alpha}_{ee} - \frac{1}{\eta_0}\hat{\alpha}_{mm}\right) E_{inc} \tag{2}$$

$$E_t = \left[1 + \frac{i\omega}{2S}\left(\eta_0 \hat{\alpha}_{ee} + \frac{1}{\eta_0}\hat{\alpha}_{mm}\right)\right] E_{inc}, \tag{3}$$

where ω is the angular frequency, S is the area of the unit cell, and η_0 is the free-space wave impedance.

Requiring $E_r = 0$ and $E_t = 0$ in equations (2-3), one can find the conditions of symmetric total absorption in a metasurface:

$$\eta_0 \hat{\alpha}_{ee} = \frac{1}{\eta_0}\hat{\alpha}_{mm} = i\frac{S}{\omega}. \tag{4}$$

By introducing the normalized polarizabilities,

$$\begin{bmatrix} \tilde{\alpha}_{ee} & \tilde{\alpha}_{em} \\ \tilde{\alpha}_{me} & \tilde{\alpha}_{mm} \end{bmatrix} = \begin{bmatrix} \eta_0 \hat{\alpha}_{ee} & \hat{\alpha}_{em} \\ \hat{\alpha}_{me} & \frac{1}{\eta_0}\hat{\alpha}_{mm} \end{bmatrix}, \tag{5}$$

(4) can be transformed into a simpler form

$$\tilde{\alpha}_{ee} = \tilde{\alpha}_{mm} = i\frac{S}{\omega}. \tag{6}$$

This means the normalized electric polarizability should be equal to the normalized magnetic polarizability. Furthermore, the electric and magnetic resonance must coincide in frequency in order to demonstrate simultaneous purely imaginary electric and magnetic polarizabilities.

The thickness of the metasurface is 17 μm, which is negligible compared to structure dimensions in the xOy plane. Therefore, omitting the z-component, $\tilde{\alpha}_{ee}$ can be expressed as:

$$\tilde{\alpha}_{ee} = \begin{bmatrix} \tilde{\alpha}_{ee}^{xx} & \tilde{\alpha}_{ee}^{xy} \\ \tilde{\alpha}_{ee}^{yx} & \tilde{\alpha}_{ee}^{yy} \end{bmatrix}, \tag{7}$$

$\tilde{\alpha}_{em}$, $\tilde{\alpha}_{me}$ and $\tilde{\alpha}_{mm}$ can be expressed similarly.

III. STABILITY ANALYSIS OF THE METAMATERIAL ABSORBER

To study the thermal stability of the absorber, an electromagnetism-thermodynamics-structural mechanics multiphysics simulation was conducted by the COMSOL Multiphysics software. The radio frequency module, the heating module and the solid mechanics module were used in the simulation.

The material of the inclusions used in the unit cell (Fig. 1) is titanium, which has a conductivity of $\sigma = 7.407 \times 10^5$S/m, a thermal expansion coefficient of 7.06×10^{-6}1/K, and a melting temperature of 1941.15 K. The unit cell is surrounded by periodic boundary conditions in the x- and y-directions. In the z-direction, the PML (Perfectly Matched Layer) boundaries are applied. In the radio frequency module, a y-polarized plane wave incidence with frequency of 2.8 THz is set to impinge from the +z direction. In the heating module, the heat source is internal Joule heat. The convective heat flux is used with a heat transfer coefficient of 10 and an initial temperature of 293.15 K (room temperature). In the solid mechanics module, one end of the straight section in the Ω ring is fixed. To be specific, the bottom end for each vertical Ω ring is fixed. For each horizontal ring, the end close to the lattice boundary is fixed.

When the incident EM power is set to be $P_{inc} = 500$W/m^2 and $P_{inc} = 10000$W/m^2, the simulated steady-state temperature is plotted in Fig. 2.

For the y-polarized incidence, only one in each Ω pair gets heated. Further simulation shows that the other

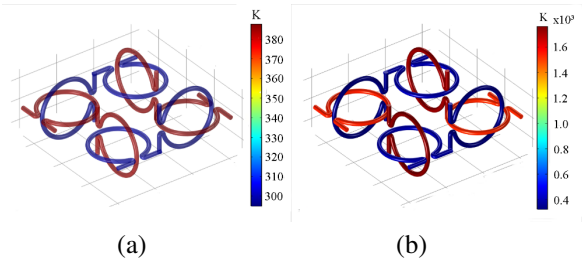

(a) (b)

Fig. 2. Corresponding temperature distribution, (a) in 500 W/m^2 and (b) in 10000 W/m^2.

half of the absorber gets heated with x-polarized incidence and is not plotted here. On each heated Ω-shaped inclusion, the heat distribution is uniform. For the P_{inc} = 500W/m^2 case, the steady temperature is 387.5 K. That temperature increases to 1761.4 K when the incident power density reaches 10000 W/m^2.

The corresponding expansion of the heated metamaterial absorber is plotted in Fig. 3. For each heated Ω ring, metallic expansion mainly occurs in the circular area.

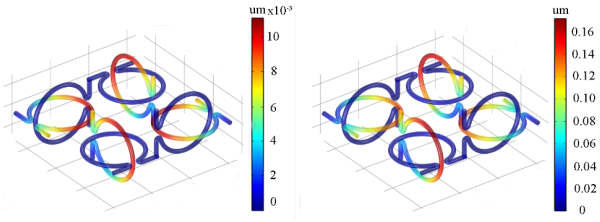

(a) (b)

Fig. 3. Corresponding displacement in different powers, (a) in 500 W/m^2 and (b) in 10000 W/m^2.

The absorption coefficient A of the absorber can be obtained from the simulated reflection coefficient R and the transmission coefficient T [21], as presented in Fig. 3.

The maximum expansion in the diameter of the Ω ring D, and the expansion rate with respect to the radius of the Ω ring (D/R) with the corresponding steady-state temperature and absorption rate are summarized in Table 1.

We can see that with a steady-state temperature of 387.5 K, the maximum expansion on the Ω ring is in the order of nanometers. For the case with a steady-state temperature of 1761.4 K, the maximum expansion is in order of 0.1 micrometer. With such expansion on the circular section, the deformation is not so big as to cause physical connection among Ω wires which might lead to dramatic change in the polarizabilities. That is why the absorption coefficient remains almost unchanged in the simulation results.

We further studied the condition that the expansion of the metal does cause the contact between the inclusions. Simulations show that only when the temperature reaches 10000 K, will the Ω particles touch each other. Taking the melting temperature of titanium (1941.15 K) into account, we arrive at the conclusion that, up to the melting temperature of the material, the absorber is thermally stable.

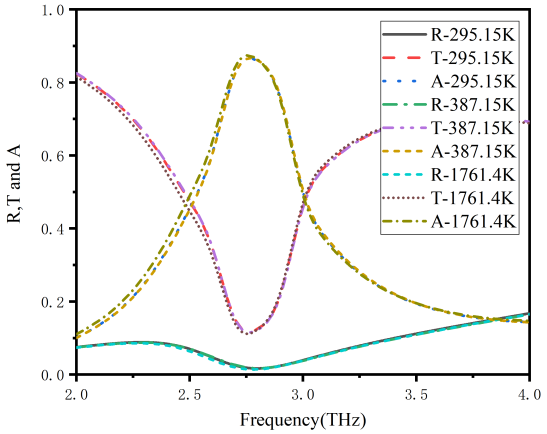

Fig. 4. Simulated reflection R, transmission T, and absorption A coefficients for the absorber, at temperature of 295.15 K, at temperature of 387.15 K and at temperature of 1761.4 K.

Table 1: Simulated peak expansion in structure and absorption at steady-state temperature

Temperature (K)	D (μm)	D/R (%)	Operating Frequency (THz)	A (%)
295.15	0	0	2.79	86.9
387.8	0.011	0.17	2.79	86.9
1761.4	0.17	2.58	2.79	86.9

IV. DESIGN AND SIMULATION RESULTS OF METASURFACE ABSORBERS

A. Design of metasurface absorbers

Based on the above thermal stability analysis, we present here the scheme to design temperature controlled metasurface absorbers by incorporating thermistors. In this scheme, the heat source may originate from the Joule heat transformed from the EM wave absorption by the Ω absorber itself, or it can be added manually through a heat conducting medium. Under this scheme, two examples are provided. As can be seen from Fig. 5, thermistors are introduced in the unit cells. In this way the functions of the metasurfaces may be dynamically controlled by temperature. Such thermistors can be realized by materials such as VO_2 [25, 26], which has an isolator phase and metallic phase with the transition temperature of around 320 K. As is shown in [25], the corresponding dynamic

range of the effective conductivity of VO_2 film is 10^1-10^5 S/m. So for the themistors, we used equivalent models of open circuits and short circuits at different temperatures.

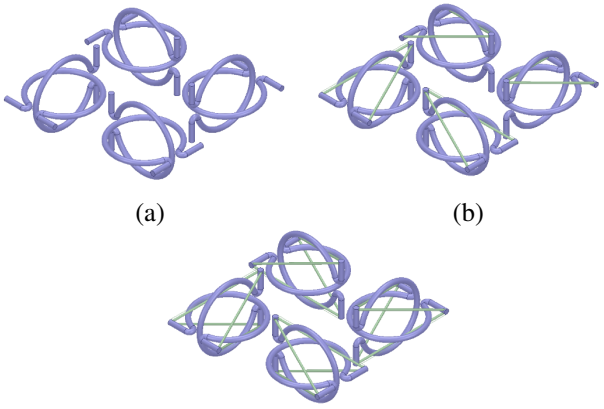

Fig. 5. Schematic of the designed absorbers, (a) Model 1, (b) Model 2, and (c) Model 3.

In the first example, 8 thermistors are added to each unit cell on one side of the Ω absorber. In the second example, 16 thermistors are added to both sides of the Ω absorber, leading to a bi-directional symmetric structure. When the temperature is 295.15 K, the resistance of thermistors is much larger compared with the resistance of titanium. So in this case, the thermistors are modelled by an open circuit. Under such a temperature, the two examples have the same equivalent models (referred to as Model 1 below) as shown in Fig. 5 (a). As the temperature rises, the resistance of the thermistors decrease and hence can be modelled by a section of aluminum as plotted in green in Figs. 5 (b) (Model 2) and (c) (Model 3), respectively.

B. Design of metasurface absorbers

From equation (6) in section II, we know that to obtain total absorption, two conditions should be satisfied. First, the normalized electric and the normalized magnetic polarizabilities of the metasurface must be equal. Second, they should be purely imaginary.

In order to validate the proposed temperature-controlled absorber designs, full-wave simulations were conducted by ANSYS High Frequency Structure Simulator (HFSS) software to evaluate the normalized polarizabilities of the proposed absorbers.

The unit cell is surrounded by periodic boundary conditions in the xOy plane, and two ports are defined in the z-direction to calculate S parameters (Fig. 6). The Ω rings can be embedded in a plastic foam substrate such as polymethacrylimide (PMI) for mechanical support [27]. This PMI material is with $\varepsilon = 1.05 - 1.13$, loss tangent

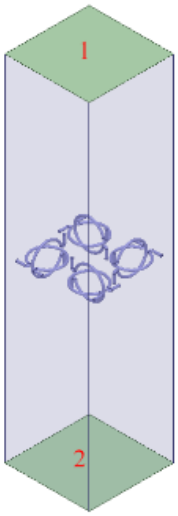

Fig. 6. Schematic of the simulation settings.

of $\delta = (1 - 18) \times 10^{-3}$, and thermal deformation temperature of 449-509 K.

Following the method in [18], the normalized polarizabilities $\tilde{\alpha}_{ee}$, $\tilde{\alpha}_{em}$, $\tilde{\alpha}_{me}$ and $\tilde{\alpha}_{mm}$ of Model 1 are obtained. Figure 7 shows that the entries on the diagonal of $\tilde{\alpha}_{ee}$ are of the order of 10^{-22}. The remaining entries are of the order of 10^{-26}. Moreover, the curves of $\tilde{\alpha}_{ee}^{xx}$ and $\tilde{\alpha}_{ee}^{yy}$ coincide. Similar results for $\tilde{\alpha}_{mm}$ can be obtained and are not plotted here. Considering the ω in equations (2) and (3) is in the order of 10^{12}, the cross-section S is in the order of 10^{-10}, the simulation results indicate that the reflected waves can be affected significantly by the diagonal elements of $\tilde{\alpha}_{ee}$ and $\tilde{\alpha}_{mm}$.

Figures 7 (c) and (d) show that all the entries of $\tilde{\alpha}_{em}$ are of the order of 10^{-26}. Similar results for $\tilde{\alpha}_{me}$ can be obtained in the same way and are not plotted here. Therefore, we can approximate the polarizability matrix as:

$$\begin{bmatrix} \tilde{\alpha}_{ee} & \tilde{\alpha}_{em} \\ \tilde{\alpha}_{me} & \tilde{\alpha}_{mm} \end{bmatrix} \simeq \begin{bmatrix} \tilde{\alpha}_{ee} & 0 \\ 0 & \tilde{\alpha}_{mm} \end{bmatrix}$$

$$= \begin{bmatrix} \begin{bmatrix} \tilde{\alpha}_{ee}^{xx} & 0 \\ 0 & \tilde{\alpha}_{ee}^{yy} \end{bmatrix} & 0 \\ 0 & \begin{bmatrix} \tilde{\alpha}_{ee}^{xx} & 0 \\ 0 & \tilde{\alpha}_{ee}^{yy} \end{bmatrix} \end{bmatrix}, \quad (8)$$

$\tilde{\alpha}_{ee}^{xx}$ and $\tilde{\alpha}_{mm}^{xx}$ are compared in Fig. 8 (a). It can be seen that $\tilde{\alpha}_{ee}^{xx}$ and $\tilde{\alpha}_{mm}^{xx}$ is close around 2.8 THz, and are almost purely imaginary. The reflection, transmission, and absorption coefficients for the metasurface in

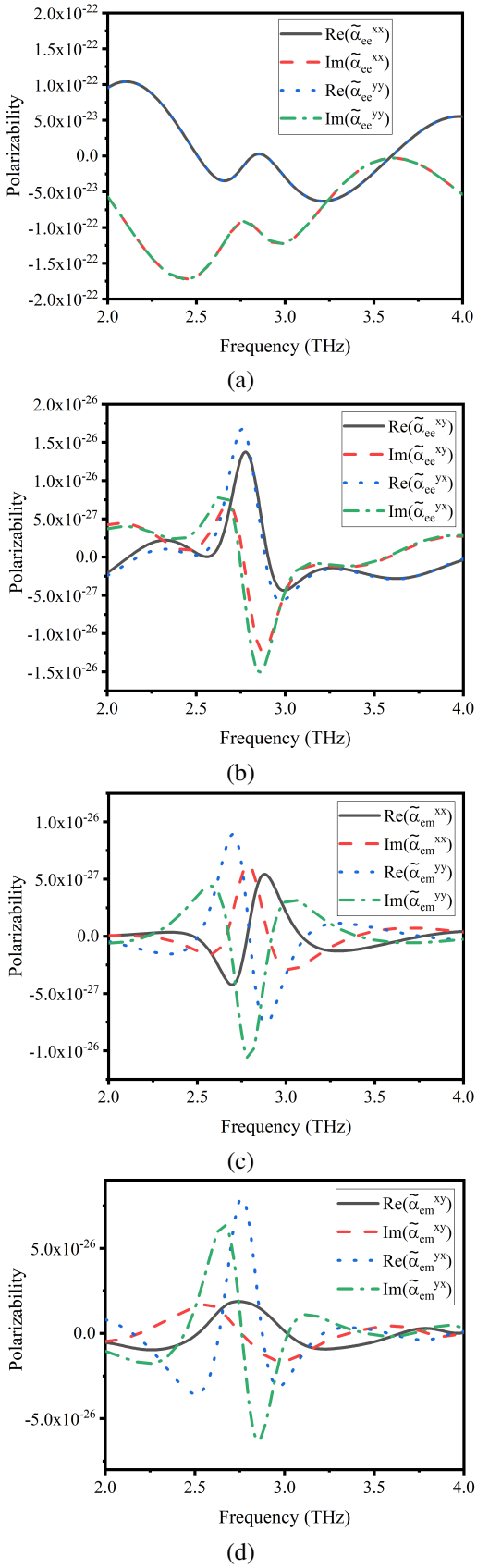

Fig. 7. The normalized polarizability results of Model 1.

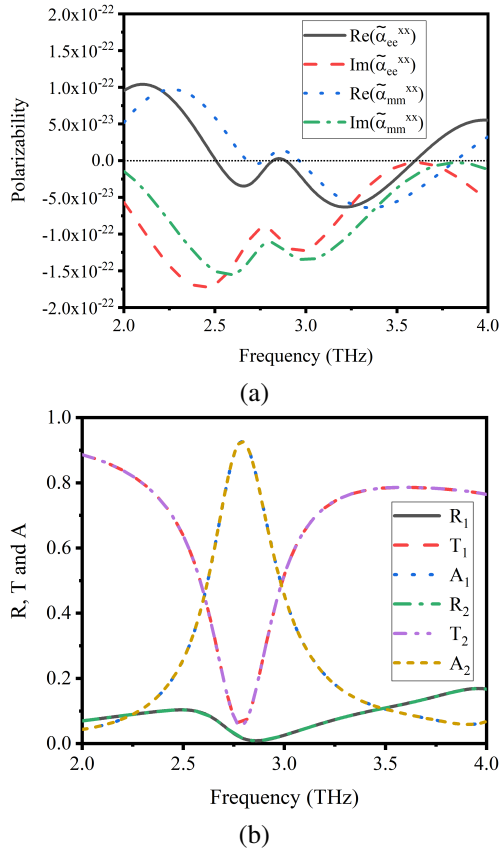

Fig. 8. The normalized polarizabilities and absorption coefficients of Model 1.

Model 1 are plotted in Fig. 8 (b). The subscript 1 or 2 corresponds to the excitation port number as defined in Fig. 6, so it indicates the direction of the incident wave. Maximum absorption coefficient of 92.7% can be seen at 2.79 THz, which agrees with the polarizability results shown in Fig. 8 (a). Since the structure bears both mirror symmetry in the z-direction and rotational symmetry in the xOy plane, the absorber functions identically for incidences from +z and -z directions, and is polarization insensitive.

The normalized polarizabilities $\tilde{\alpha}_{ee}$, $\tilde{\alpha}_{em}$, $\tilde{\alpha}_{me}$ and $\tilde{\alpha}_{mm}$ of Model 2 can also be obtained. Similarly to Model 1, the normalized polarizabilities of Model 2 can also be approximated by equation (8).

Comparing $\tilde{\alpha}_{ee}^{xx}$ and $\tilde{\alpha}_{mm}^{xx}$ plotted in Fig. 9 (a), we can see around 3.5 THz $\tilde{\alpha}_{ee}^{xx}$ and $\tilde{\alpha}_{mm}^{xx}$ are close and are almost purely imaginary. Correspondingly, peak absorptions occur around this frequency (Fig. 9 (b)). This metasurface is still polarization insensitive. However, since the structure loses the mirror symmetry in the z-direction, a slight difference in A_1 and A_2 can be observed, indicating the metasurface functions differently for the upward and the downward incidences.

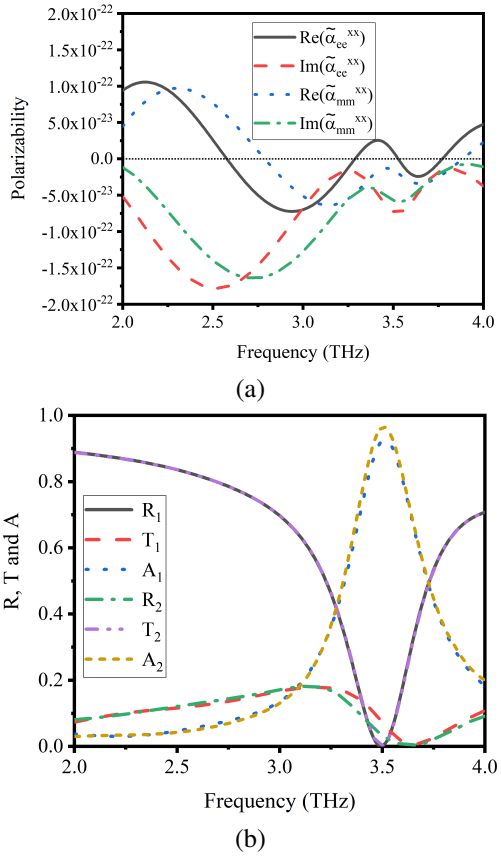

Fig. 9. The normalized polarizabilities and absorption coefficients of Model 2.

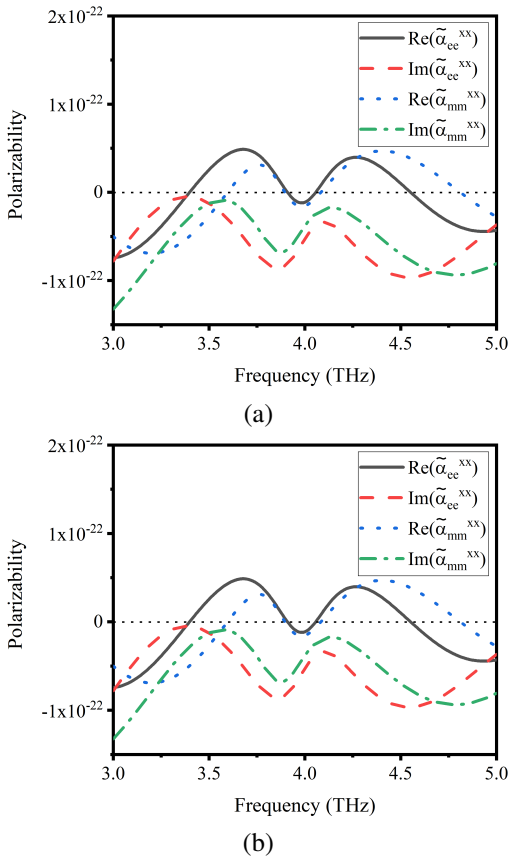

Fig. 10. The normalized polarizabilities and absorption coefficients of Model 3.

Specifically, the absorption coefficient changes from 92.5% (at 3.52 THz) to 96.7% (at 3.51 THz) when the incident direction changes from -z to +z.

Similar conclusions can be drawn with Model 3. The normalized polarizabilities $\tilde{\alpha}_{ee}$, $\tilde{\alpha}_{em}$, $\tilde{\alpha}_{me}$ and $\tilde{\alpha}_{mm}$ of Model 3 are similar with Model 1, in which polarizabilities can be approximated by equation (8).

$\tilde{\alpha}_{ee}^{xx}$ and $\tilde{\alpha}_{mm}^{xx}$ is close around 4.0 THz, and are almost purely imaginary (Fig. 10 (a)). Accordingly, peak absorption of 93.8% can be found at 3.94 THz (Fig. 10 (b)). Due to its structural symmetry, the absorber in this model is polarization insensitive and bi-directional.

To sum up, the above investigation validates the thermal controlling of the absorbing frequencies, with the overall absorption coefficients of over 90%.

C. Effective circuit analysis

The operation of the proposed temperature controlled absorbers can be understood by equivalent circuit models. In this section, we used the commercial software of Advanced Design System (ADS) to perform the circuit analysis. Through the structure analysis, we can determine the equivalent circuit, as shown in Fig. 11,

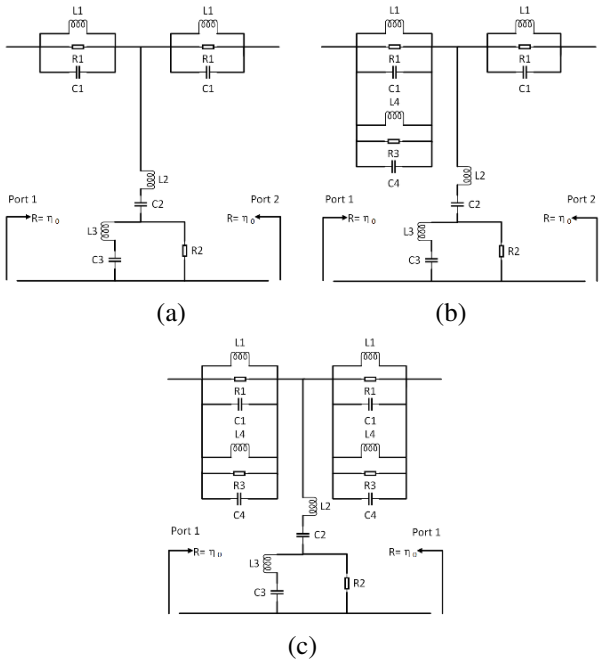

Fig. 11. Schematic of effective circuits, (a) Model 1, (b) Model 2, and (c) Model 3.

whose parameters can be further approximated through optimization.

The equivalent circuit models for Models 1 to 3 are plotted in Fig. 11. Due to the z-directional symmetry in the physical structures, models in Figs. 11 (a) and (c) demonstrate corresponding port symmetry. $\eta_0$stands for the wave impedance in free space. The parameters are summarized in Table 2.

Table 2: Parameters of the equivalent circuit models

Model	a	b	c
L1 (pH)	1.05	1.05	1.05
L2(pH)	0.002	0.002	0.002
L3(pH)	1.93	1.93	1.93
L4(pH)	-	0.42	0.42
C1 (pF)	0.003	0.003	0.003
C2 (pF)	0.0003	0.0003	0.0003
C3 (pF)	8.42	8.42	8.42
C4 (pF)	-	0.002	0.002
R1(Ω)	377	377	377
R2(Ω)	17	17	17
R3(Ω)	1288.7	1288.7	1288.7

The simulation results of HFSS and ADS for the three models are compared in Fig. 12. As in Figs. 8–10, the subscript indicates the port of excitation. It can be seen that the ADS and HFSS simulation results agree well at the absorption frequencies for all the models, which validates the effective circuit models. We can also see that the HFSS models have broader absorption frequency bands than the ADS models. The reason is that the circuit models have fewer degrees of freedom, leading to stronger sensitivity to frequency. If a more complex circuit model design could be adopted,

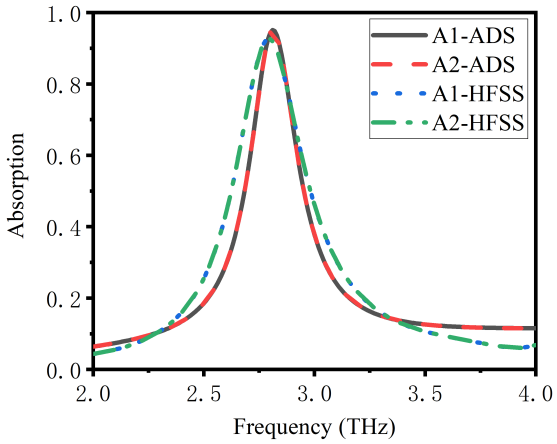

(a)

Fig. 12. *Continued*

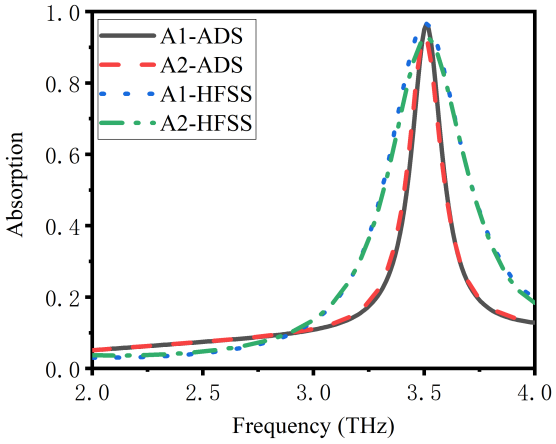

(b)

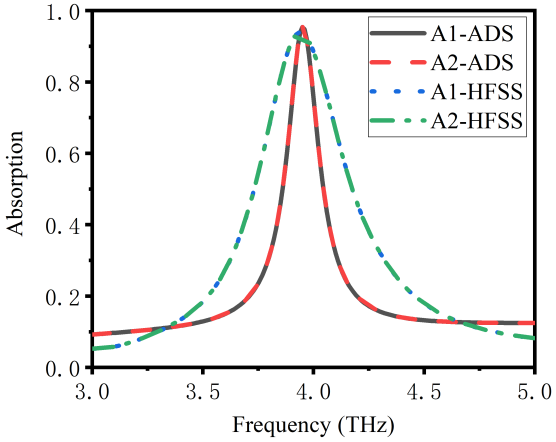

(c)

Fig. 12. Simulated absorption coefficients, (a) Model 1, (b) Model 2, and (c) Model 3.

the results, it would be suggested, would be more consistent.

V. CONCLUSION

In this study, we analyzed the stability of an Ω-shaped absorber and designed two temperature-controlled EM absorbers based on electromagnetism-thermodynamics-structural mechanics multiphysics simulation. Up to the temperature of 1761.4 K, which is close to the melting temperature of the material, the expansion of the Ω-shaped inclusion is within the order of 0.1 μm with expansion rate of no greater than 2.58%. The absorption coefficient maintained at 92.7% at 2.79 THz. This demonstrated the thermal stability of the Ω absorber both in structure and in EM wave absorption function. By adding thermistors, two temperature-controlled absorbers were designed. When the temperature rises, the simulated absorption of the two proposed absorbers demonstrated a frequency shift from 2.79 THz to 3.51 (+0.01) THz and 3.94 THz, with corresponding absorption coefficients of 92.5 (+4.2)%

and 93.8%, respectively. At the end of the paper, the effective circuit model method is used to analyze the two metasurface absorbers. In the THz frequency regime, the proposed thermal-controlled absorbers have substantial potential for being used for spatial light modulators, sensors, and bolometers.

REFERENCES

[1] Y. P. Hong, I. J. Hwang, D. J. Yun, D. J. Lee, and I. H. Lee, "Design of single-layer metasurface filter by conformational space annealing algorithm for 5G mm-wave communications," *IEEE Access*, vol. 9, pp. 29764-29774, Feb. 2021.

[2] W. L. Guo, G. M. Wang, H. P. Li, K. Zhang, and T. Cai, "Ultra-thin two-dimensional transmissive anisotropic metasurfaces for polarization filter and beam steering application," *Chinese Physics B*, vol. 25, no. 10, pp. 104101-104107, Oct. 2016.

[3] Z. Zhang, Y. Zhang, T. Wu, S. Chen, W. Li, and J. Guan, "Broadband RCS reduction by a quaternionic metasurface," *Materials*, vol. 14, no. 11, pp. 2787-2797, May 2021.

[4] Y. Saifullah, F. Zhang, G. Yang, and F. Xu, "3-bit polarization insensitive reflective metasurface for RCS reduction," *The 12th International Symposium Antennas, Propagation, and EM Theory (ISAPE 2018),* Hang Zhou, China, pp. 1-3, Dec. 2018.

[5] C. Huang, W. Pan, X. Ma, and X. Luo, "Wideband radar cross-section reduction of a stacked patch array antenna using metasurface," *IEEE Antennas and Wireless Propagation Letters*, vol. 14, pp. 1369-1372, Dec. 2015.

[6] T. A. Khan, J. Li, U. Raza, J. Chen, and A. Zhang, "Design of a metasurface with wide RCS reduction bandwidth," *2019 Photonics & Electromagnetics Research Symposium - Fall (PIERS - Fall),* Xiamen, China, pp. 976-982, Dec. 2019.

[7] T. Almoneef and O. M. Ramahi, "Dual-polarized multi-band infrared energy harvesting using h-shaped metasurface absorber," *Progress in Electromagnetics Research C*, vol. 76, pp. 1-10, Jan. 2017.

[8] N. Muhammad, T. Fu, Q. Liu, X. Tang, Z. L. Deng, and Z. Ouyang, "Plasmonic metasurface absorber based on electro-optic substrate for energy harvesting," *Materials*, vol. 11, pp. 2315-2325, Nov. 2018.

[9] M. Bağmancı, M. Karaaslan, E. Ünal, O. Akgol, F. Karadağ, and C. Sabah, "Broad-band polarization-independent metamaterial absorber for solar energy harvesting applications," *Physica E: Low-dimensional Systems and Nanostructures,* pp. 1-6, June 2021.

[10] A. Kumar, C. Saha, and R. Sethunadh, "Dual band energy harvester based on metasurface absorber," *2020 URSI Regional Conference on Radio Science (URSI-RCRS),* Varanasi, India, pp. 1-4, Feb. 2020.

[11] K. Zhang, Y. Wang, S. N. Burokur, and Q. Wu, "Generating dual-polarized vortex beam by detour phase: From phase gradient metasurfaces to metagratings," *IEEE Transactions on Microwave Theory and Techniques*, vol. 70, no. 1, pp. 200-209, Jan. 2022.

[12] Y. Yuan, S. Sun, Y. Chen, K. Zhang, and C. Qiu, "A fully phase-modulated metasurface as an energy-controllable circular polarization router," *Advanced Science*, vol. 7, no. 18, pp. 2001437, July 2020.

[13] X. Zhang, H. Liu, Z. Zhang, Q. Wang, and S. Zhu, "Controlling thermal emission of phonon by magnetic metasurfaces," *Scientific Reports*, vol. 7, no. 1, pp. 1-8, Feb. 2017.

[14] J. Li, B. Yu, and S. Shen, "Scale law of far-field thermal radiation from plasmonic metasurfaces," *Physical Review Letters*, vol. 124, no. 13, pp. 137401, Mar. 2020.

[15] Y. Ueba and J. Takahara, "Spectral control of thermal radiation by metasurface with split-ring resonator," *Applied Physics Express*, vol. 5, no. 12, pp. 122001, Dec. 2012.

[16] T. Niemi, A. O. Karilainen, and S. A. Tretyakov, "Synthesis of polarization transformers," *IEEE Transactions on Antennas and Propagation*, vol. 61, no. 6, pp. 3102-3111, June 2013.

[17] X. X. Liu, Y. Zhao, and A. Alù, "Polarizability tensor retrieval for subwavelength particles of arbitrary shape," *IEEE Transactions on Antennas and Propagation*, vol. 64, no. 6, pp. 2301-2310, June 2016.

[18] M. Yazdi and N. Komjani, "Polarizability calculation of arbitrary individual scatterers, scatterers in arrays, and substrated scatterers," *JOSA B*, vol. 33, no. 3, pp. 491-500, 2016.

[19] L. Pulido-Mancera, P. T. Bowen, M. F. Imani, N. Kundtz, and D. Smith, "Polarizability extraction of complementary metamaterial elements in waveguides for aperture modeling," *Physical Review B*, vol. 96, no. 23, pp. 235402-235404, Mar. 2017.

[20] V. S. Asadchy, I. A. Faniayeu, Y. Ra'Di, S. Khakhomov, I. Semchenko, and S. Tretyakov, "Broadband reflectionless metasheets: frequency-selective transmission and perfect absorption," *Physical Review X*, vol. 5, no. 3, pp. 031005-031007, July 2015.

[21] A. Balmakou, M. Podalov, S. Khakhomov, D. Stavenga, and I. Semchenko, "Ground-plane-less bidirectional terahertz absorber based on omega resonators," *Optics Letters*, vol. 40, no. 9, pp. 2084-2087, Sep. 2015.

[22] C. M. Watts, D. Shrekenhamer, J. Montoya, G. Lipworth, J. Hunt, and T. Sleasman, "Terahertz compressive imaging with metamaterial spatial light modulators," *Nature Photonics*, vol. 8, no. 8, pp. 605-609, Aug. 2014.

[23] M. Gustafsson, I. Vakili, S. E. B. Keskin, D. Sjoberg, and C. Larsson, "Optical theorem and forward scattering sum rule for periodic structures," *IEEE Transactions on Antennas and Propagation*, vol. 60, no. 8, pp. 3818-3826, Aug. 2012.

[24] K. N. Rozanov, "Ultimate thickness to bandwidth ratio of radar absorbers," *IEEE Transactions on Antennas and Propagation*, vol. 48, no. 8, pp. 1230-1234, Aug. 2000.

[25] H. Liu, J. Lu, and X. R. Wang, "Metamaterials based on the phase transition of VO2," *Nanotechnology*, vol. 29, no. 2, pp. 024002-024003, Jan. 2017.

[26] A. M. Shaltout, V. M. Shalaev, and M. L. Brongersma, "Spatiotemporal light control with active metasurfaces," *Science*, vol. 364, pp. 648-657, May 2019.

[27] F. Zhao, "Present state of art of polymethacrylimide (PMI) foam research," *Aerospace Materials and Technology*, pp. 1-6, Jan. 2008.

[28] J. Li and J. Dho, "Characteristics of phase transition of VO2 films grown on TiO2 substrates with different crystal orientations," *Journal of Crystal Growth*, vol. 404, pp. 84-88, July 2014.

Jia-Tong Jing received his B.E. and M.S. degrees from the Beijing Institute of Technology, Beijing, China, in 2018 and 2021 respectively. He is currently pursuing a Ph.D. degree at the Institute of Radio Frequency Technology and Software from Beijing Institute of Technology. His current research interests include metamaterial and computational electromagnetics.

Wei Song received her B.S. degree from North Eastern University, Shen-yang, China, in 2002, and her M.S. and Ph.D. degrees from Queen Mary University of London, London, UK, in 2003 and 2008, respectively. She is currently an Associate Professor with the School of Information and Electronics, Beijing Institute of Technology, Beijing, China. She has authored or co-authored over 20 papers in refereed journals and international conferences, and has co-authored a monograph in computational electromagnetics. Her current research interests include high-performance methods in computational electromagnetics, EM property analysis, and metamaterial-based antenna design.

Ting-Ting Ge received her B.E. degree from North China University of Technology, Beijing, China, in 2019, and her M.S. degree from the Beijing Institute of Technology, Beijing, China, in 2022. Her current research interests include EM property analysis, and metamaterial-based antenna design.

Xin-Qing Sheng received his B.S., M.S. and Ph.D. degrees from the University of Science and Technology of China (USTC), Hefei, China, in 1991, 1994, and 1996, respectively. Sheng is a Chang-Jiang Professor of the School of Information and Electronics at the Beijing Institute of Technology. Sheng has authored and co-authored over 150 papers in refereed journals, and three books: *Essentials of Computational Electromagnetics* (Singapore: IEEE Press-Wiley, 2012), *A Brief Treatise on Computational Electromagnetics* (Beijing: Science Press, 2004), and *A Treatise on Electromagnetic Waves* (Beijing: Science Press, 2007). Sheng authored SINOCOM, a simulation software for scattering by complex targets. His research interests include computational electromagnetics, scattering and antenna analysis, electromagnetic compatibility, and microwave imaging.